Local conductivity and surface photovoltage variations due to magnesium segregation in *p*-type GaN

B. S. Simpkins and E. T. Yu[a)]
Department of Electrical and Computer Engineering and Program in Materials Science and Engineering, University of California at San Diego, La Jolla, California 92093-0407

U. Chowdhury, M. M. Wong, T. G. Zhu, D. W. Yoo, and R. D. Dupuis
Microelectronics Research Center, The University of Texas at Austin, Austin, Texas 78712

(Received 9 February 2004; accepted 1 March 2004)

Conductive atomic force microscopy (C-AFM) and surface photovoltage (SPV) microscopy were used to investigate local electronic structure in *p*-type GaN. C-AFM imaging revealed locally reduced forward- and reverse-bias conductivity near threading dislocations. In addition, regions near threading dislocations demonstrated significantly enhanced surface photovoltage response when compared to regions away from dislocations. Analytical treatment of the surface photovoltage as a function of pertinent material properties indicated that reduced background dopant concentration is the most likely cause for the increased SPV. Both reduced conductivity and enhanced surface photovoltage are shown to be consistent with Mg segregation to dislocation cores that results in regions of locally decreased electrically active Mg concentration surrounding the dislocations. [DOI: 10.1063/1.1713025]

I. INTRODUCTION

Great advances have been made in the development and utilization of GaN-based materials for optoelectronic and electronic devices. However, the performance of optical devices and of nitride-based bipolar transistors would benefit from an improved understanding of issues relevant to *p*-type conductivity in GaN. Unfortunately, the most widely used *p*-type dopant in GaN, magnesium, suffers from high activation energy,[1] susceptibility to passivation via the formation of H defect complexes,[2] and the tendency to produce structural defects such as inclusions and even polarity inversion.[3] It is therefore of great technological and scientific importance to investigate the nature of Mg incorporation in GaN and the resulting nanoscale electronic behaviors.

Previous studies of Mg incorporation in GaN have shown a plateau in free hole concentration with increased Mg incorporation,[4] suggesting the formation of hole-passivating defects at high Mg concentrations, although this critical fraction of Mg is likely dependent on growth parameters. Nearly all studies of the electronic properties of *p*-type GaN have been conducted on large-scale device structures, and are therefore largely insensitive to microscale and nanoscale variations in electrical behavior that may exist. Previous surface photovoltage measurements on GaN-based materials have either examined the average behavior of large surface areas[5] or studied response at only one point on the surface.[6] Because spatially resolved analysis is impossible in such experiments, characterization of electrical behavior at the nanoscale may be highly illuminating. TEM-based structural investigations[7] of Mg-doped GaN suggest that Mg may segregate to dislocation cores, leaving a Mg-deficient region surrounding the dislocation; however, there have been no complementary studies to evaluate the impact of Mg segregation on local electronic properties. Examination of electrical properties such as conductivity and dopant concentration with high spatial resolution will help elucidate the relationship between electronic behaviors and structural defects, and thereby provide insight into the issues most relevant to improving *p*-type conductivity and device performance.

In the present study, we have employed conductive atomic force microscopy (C-AFM) combined with scanning Kelvin probe (SKP) and surface photovoltage (SPV) microscopies to evaluate conductivity, surface potential, and photovoltage variations, respectively, along with their correlation to structural defects. Our results reveal a correlation between regions of both reduced conductivity and increased SPV and the presence of threading dislocations. An analytical treatment of the SPV response provided insight into the origin of the conductivity and SPV variations.

II. EXPERIMENT

The sample structure employed in these studies was grown by low-pressure metalorganic chemical vapor deposition (MOCVD) in an Emcore D125 UTM reactor. Growth pressure was 50 Torr for AlN and 200 Torr for GaN under a hydrogen shroud with a V-III ratio in excess of 3000. The precursors used were trimethylaluminum (TMAI), trimethylgallium (TMGa), ammonia (NH_3), silane (SiH_4), and biscyclopentadienylmagnesium (Cp_2Mg). Initially, a high-temperature (~1070 °C) AlN buffer layer of 100 nm thickness was grown on a *c*-plane 6H-SiC substrate, and the subsequent *p*- and *n*-type GaN layers were grown at ~1050 °C. These subsequent layers include an undoped template layer, highly and moderately doped *n*-type regions, and finally, a 150 nm thick *p*-type layer. A schematic of the sample structure, including dopant concentrations, layer

a)Electronic mail: ety@ece.ucsd.edu

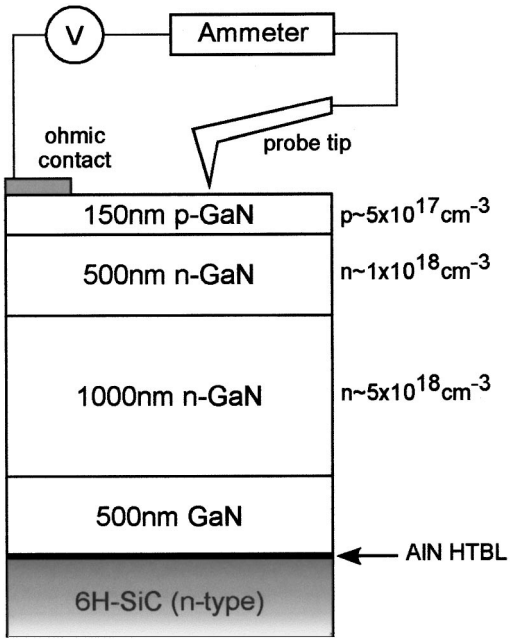

FIG. 1. Schematic of sample structure and conductive AFM configuration.

thicknesses, and the experimental geometry, is shown in Fig. 1. The full width at half maximum of the (102) x-ray diffraction rocking curve for the sample studied was ~300 in. Secondary ion mass spectrometry measurements yield a Mg concentration of $\sim 3\times 10^{19}$ cm^{-3}. A free hole concentration of $\sim 5\times 10^{17}$ cm^{-3} and a mobility of ~10 cm^2/V s were obtained from room temperature Hall measurements performed on calibration samples grown under the same conditions.

Local conductivity and surface potential measurements were carried out in a modified Digital Instruments Nanoscope® IIIa MultiMode™ microscope under ambient atmospheric conditions (~20 °C with 50% relative humidity). The C-AFM technique has been described previously.[8] Briefly, a highly doped diamond-coated tip is held in contact with the sample surface and acts as a Schottky contact to the sample. While scanning in contact mode, forward- (reverse-) bias conditions are established through the application of a positive (negative) bias to an ohmic contact on the *p*-type sample surface and the current through the tip is measured with a current amplifier; in this manner, correlated topographyic and current images are obtained. This technique reveals variations in conductivity with a spatial resolution of tens of nanometers, limited by tip radius.

SKP and SPV microscopies utilize a conductive Co-Cr coated tip operated in lift mode. In scanning Kelvin probe microscopy, after acquiring each line of topographic data, the tip is lifted by a prescribed distance (30 nm in this experiment) and rescanned over the same region, maintaining a constant tip-sample separation. Tip-sample force during this lifted line scan is minimized through the application of a dc ''nulling bias.'' [9] This bias voltage is adjusted via a feedback loop acting to minimize the tip oscillation amplitude, which is proportional to tip-sample force.[10] The bias voltage at which the force component at the oscillation frequency is minimized corresponds to the tip-sample contact potential

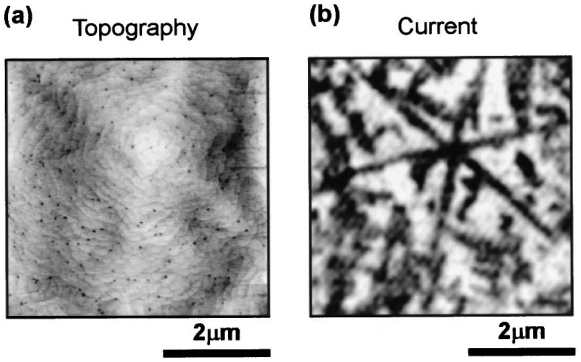

FIG. 2. (a) Topographic and (b) current images of a 5 μm$\times$5 μm area. Surface pits in (a) yield a dislocation density of $(7-10)\times 10^8$ cm^{-2}. Dark areas in (b) correspond to decreased reverse-bias current and correlate to the ridges emanating radially from the peak seen just above center in (a). Gray scales correspond to (a) 8 nm and (b) 10 pA.

and thus provides a measure of the relative surface potential. Spatial resolution is dependent on the tip size, lift height, and nature of the electrostatic force interaction.

In surface photovoltage microscopy, modulation of the surface potential of a semiconductor through incident illumination[11] is imaged. Super-band-gap photons incident on the sample generate electron-hole pairs, which redistribute themselves according to the electric fields present near the semiconductor surface. Fields near a depleted surface will draw minority carriers toward the surface. In this manner, photogenerated minority carriers partially screen surface-state charges and thereby reduce the surface depletion charge needed to maintain charge neutrality, resulting in a decrease in surface band bending. In *p*-type material, a decrease in surface band bending corresponds to a decrease in the surface potential as measured by scanning Kelvin probe. Therefore, the shift in surface potential due to illumination, termed the SPV, is negative for *p*-type material. Regions exhibiting a larger negative surface potential shift will be referred to as having a larger SPV. In the present study, illumination which includes super-band-gap components is incident onto the sample surface while the spatial distribution of the SPV is monitored using the previously described Kelvin probe method and correlated with conductivity variations and defect locations.

III. RESULTS AND DISCUSSION

The results and discussion are presented in three sections. First, topographic and conductivity data, as well as correlations of electrical conductivity with dislocations, will be discussed. Equilibrium (SKP) and illuminated (SPV) surface potential measurements will then be presented. Finally, the SPV effect will be treated analytically, and an explanation proposed for the correlation of the local conductivity and SPV variations with the spatial distribution of dislocations.

A. Local conductivity measurements

Simultaneously acquired topographic and current images are presented in Figs. 2(a) and 2(b), respectively. Atomic ledges, ~0.4 nm high and indicative of the step flow growth

mode,[12] and surface pits, ~2 nm deep with radii of 25–50 nm, are visible in Fig. 2(a). The surface pits are most likely due to the intersection of threading dislocations with the surface.[12] Surface pits in GaN have previously been associated with dislocations[13,14] and the density of observed pits, $(7-10)\times 10^8$ cm^{-2}, is consistent with the dislocation density for this sample as measured by TEM.[15] Reverse-bias current variations, measured with an applied bias voltage $V_{\text{sample}} = -10$ V, are shown in Fig. 2(b), with regions of decreased current magnitude appearing dark. The magnitude of the overall current and of the observed variations in current is several picoampere. It is evident from the figure that some—although not all—regions of reduced current magnitude exhibit sixfold symmetry. These regions generally appear to follow the ridges emanating radially from the center of growth mounds, as seen in Fig. 2(a), and likely lie in $\langle 11\bar{2}0\rangle$ type directions.[16] Similar conductivity variations are observed under forward-bias conditions (not shown); regions exhibiting decreased reverse-bias current also exhibit decreased forward-bias current.

Although topographic variations can influence the C-AFM measurement through the variation of the tip-sample contact area, and thus the contact resistance, only topographic variations occurring on the length scale of the tip, such as an atomic step edge, would be expected to affect contact area. The sixfold symmetric C-AFM features referred to above do appear to follow the ridges in the topography as previously discussed; however, at 200–500 nm, the lateral length scale of these topographic variations is large compared to the tip size, typically ~20 nm. Consequently, these regions appear essentially flat to the tip and do not influence contact resistance or current. Topographically induced artifacts may therefore be ruled out as the cause of these current variations and crystallographic causes may be explored.

Threading dislocations in GaN-based materials can be electrically active and have been found to cause carrier scattering[17] and locally decreased electrostatic potential[18] due to charge trapping at the dislocation core. The correlation between conductivity variations and dislocations is presented in Fig. 3. The locations of surface pits in the topographic scan of Fig. 3(a) are marked as open circles in the current image of Fig. 3(b). There is a clear correlation between surface pits, which correspond to threading dislocations, and regions of decreased conductivity. Previous studies have correlated highly conductive current paths with screw dislocations in *n*-type GaN grown under certain conditions.[8,19] However, to our knowledge locally decreased conductivity associated with dislocations has never been observed. Several possibilities could account for this variation in conductivity, including doping or surface barrier variations, or electrically active dislocations trapping carriers leading to local depletion. Free-carrier[13] and surface barrier[18] variations have been found to be associated with threading dislocations in *n*-type material as acceptor-type trap states within dislocations become occupied leading to decreased potential and local depletion; however, acceptor traps near midgap would likely not become charged in the *p*-type material investigated in the present study. Local probing of complimentary electronic properties, specifically equilibrium surface potential and photovoltage response, was therefore performed in an effort to reveal the mechanisms responsible for the observed reduced conductivity near dislocations.

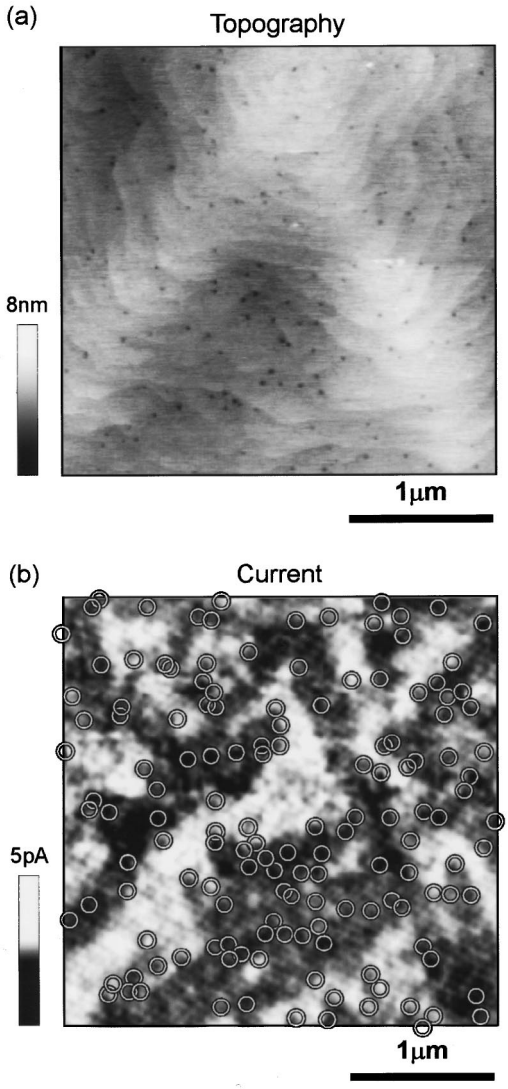

FIG. 3. (a) Topographic and (b) current images of a 3 μm$\times$3 μm area, with open circles in (b) indicating dislocation positions. The dislocations occur primarily in the dark (low current) regions of (b), indicating that the presence of dislocations reduces conductivity.

B. Surface potential and photovoltage measurements

Scanning Kelvin probe microscopy is sensitive to surface potential variations, which can be caused by charged dislocations; however, equilibrium SKP measurements indicated that surface potential variations were minimal in the *p*-type GaN material studied here. Figures 4(a) and 4(b) show SKP images for equilibrium and illuminated conditions, respectively. At equilibrium, surface potential variations of ~5 meV in amplitude were observed—near the noise level of the instrument (~1 meV). This result indicated that dislocations in these samples were either uncharged, or charged but screened by a very high density of surface states. Illumination with super-band-gap photons, however, had a pronounced effect on the surface potential. Figure 4(b)

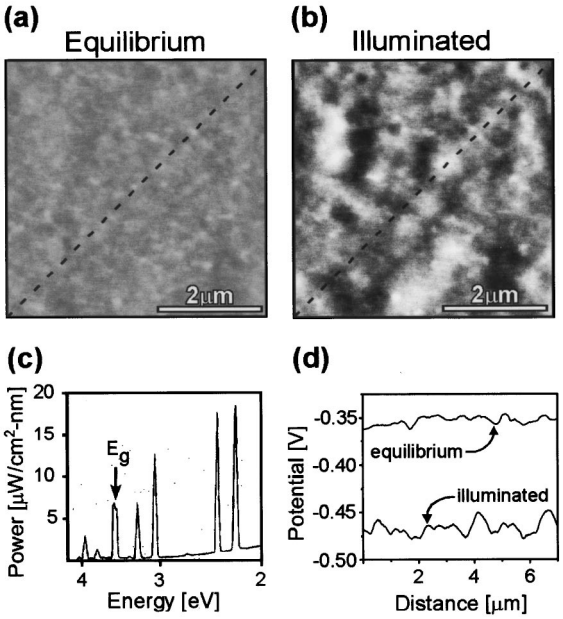

FIG. 4. Surface potential images obtained under (a) equilibrium and (b) illuminated conditions. The illumination spectrum is shown in (c). (d) Profiles taken along the diagonal lines indicated in images (a) and (b). Illumination reduces the overall surface potential and increases the magnitude of surface potential variations.

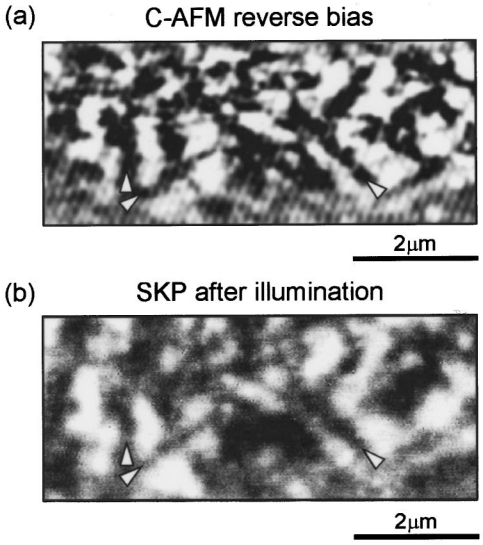

FIG. 5. (a) Current and (b) postillumination surface potential images of a 7 μm$\times$3 μm area. White arrowheads have been placed in corresponding regions of (a) and (b) to facilitate observation of correlated behaviors.

shows a surface potential image acquired after the sample was illuminated with a mercury lamp source having the spectral distribution plotted in Fig. 4(c). The most striking effect of the illumination was the increase in contrast amplitude, clearly visible in Fig. 4(b), from which we deduced that certain regions exhibited a greater SPV than other regions. In addition to an increase in spatial variation of the surface potential, the average potential of the entire surface experienced a decrease upon illumination. Unprocessed section profiles were extracted for the equilibrium and illuminated scans and are plotted in Fig. 4(c). These sections, taken along the diagonal dashed lines in Figs. 4(a) and 4(b), showed that the overall surface potential is reduced by ~120 mV due to illumination.

An overall decrease in surface potential upon superband-gap illumination is expected for *p*-type material. Upon illumination, photogenerated minority carriers (electrons for *p*-type material) are swept toward the surface by the electric field within the surface depletion layer. These carriers increase the negative charge density near the surface, thereby increasing the potential energy for electrons near the surface and correspondingly decreasing the degree of surface band bending present.[11] The dark regions visible in Fig. 4(b) exhibited a larger negative shift in surface potential upon illumination and are therefore referred to as having larger SPV.

The spatial correlation between local variations in SPV and in conductivity was examined to investigate the origin of these local electronic behaviors and is shown in Figs. 5(a) and 5(b), in which C-AFM and postillumination SKP images of a single area are displayed. The dark regions in Fig. 5(a), corresponding to decreased current magnitude, correlate very closely with the dark regions in Fig. 5(b), which correspond to larger SPV response. White arrowheads have been placed in each image to indicate correlated dark regions in both scans. These results clearly demonstrate that regions exhibiting decreased conductivity also exhibit increased SPV response. Recalling that regions of reduced current were also associated with the presence of dislocations, we therefore associate the presence of dislocations with both decreased current and increased SPV. A direct comparison between SPV features and dislocation positions was less revealing because SPV features were larger and more diffuse than C-AFM features. Several factors affect the spatial resolution of surface potential measurements, including the tip-sample separations of several tens of nanometers, sensitivity to long-range electrostatic forces, and photogenerated carrier diffusion, limiting the spatial resolution of this technique to 100–300 nm for the conditions used.[20] C-AFM measurements, on the other hand, are made with the tip in contact with the sample, resulting in a spatial resolution ultimately limited by the tip size, typically 10–50 nm in radius.

Thus dislocations, which were previously correlated with regions of decreased conductivity, are also correlated with regions that exhibited a larger SPV response. To understand the physical origin of these correlations requires an examination of the dependence of SPV and conductivity on material parameters. Factors that may lead to nonuniform SPV include variations in initial surface band bending, surface-state density, surface-state energy position, generation-recombination rates, and doping. Variations in the initial band bending or surface-state density and energy position are not likely to be present in these samples. These factors would lead to spatial variations in the equilibrium surface potential, which, as shown in Fig. 4(a), are not observed. Spatial variation in generation-recombination rates, which would effectively amount to a change in the density of photoinduced carriers, is also not likely if the dominant photoionization processes are band-to-band transitions. Photoionization of defect states within the band gap may be

neglected for illumination energies even slightly (~0.01 eV) above the band gap;[21] however, the illumination source used in the present study did include sub-band-gap components, which may influence minority carrier generation. A region with an increased density of a particular gap state would experience a reduced net recombination rate, longer minority carrier lifetimes, and therefore, increased minority carrier injection in that region. Sub-band-gap transitions related specifically to Mg point defects could influence SPV response, but an increased concentration of Mg-related point defects near dislocations, leading to the observed increased SPV, would not be consistent with the local conductivity results of the current study or the TEM results in Ref. 7 and was, therefore, considered unlikely. Transitions involving other midgap trap states, such as electron promotion from the valence band into gap states, were possible but charge redistribution would also be required in order to effect a change in the surface potential and trap-to-trap hopping is not expected to be an efficient transport mechanism. Also, the density of bulk point defects is expected to be significantly lower than the valence and conduction band effective densities of states, 4.6×10^{19} cm^{-3} and 2.2×10^{18} cm^{-3}, respectively, and therefore should make a significantly smaller contribution to the SPV than band-to-band transitions.[11] The remaining factor was then local variation in acceptor concentration near dislocations. The influence of doping on SPV was therefore examined analytically and is presented in the following section.

C. Analysis of photovoltage response

The SPV effect and the material parameters affecting photovoltage response have been previously examined in detail.[11] SPV response may be treated analytically beginning with the charge neutrality condition,

$$Q_{ss}+Q_{sc}=0, \tag{1}$$

where Q_{ss} and Q_{sc} are the equilibrium surface-state charge and the surface depletion space charge per unit area, respectively. Under the nonequilibrium conditions induced by illumination, charge neutrality will still hold; however, we will use the superscript* to denote nonequilibrium properties, i.e., $Q_{ss}^*+Q_{sc}^*=0$. Assuming that the quasi-Fermi levels throughout the depletion region are flat during illumination, an assumption appropriate for depleted surfaces of reasonable quality with carrier excitation uniform throughout the space charge region,[22] the total space charge may be integrated, from which the surface depletion region charge per area under illumination is given by[11]

$$Q_{sc}^*=\mp\frac{\sqrt{2}\varepsilon_s kT}{eL_d}\left[\left(e^{-eV^*/kT}+\frac{eV^*}{kT}-1\right)+\frac{n_b}{p_b}\left(e^{eV^*/kT}-\frac{eV^*}{kT}-1\right)+\frac{n_b}{p_b}\Delta_a(e^{-eV^*/kT}+e^{+eV^*/kT}-2)\right]^{1/2}, \tag{2}$$

where L_d is the Debye screening length, V the surface potential measured from the bulk Fermi level, n_b and p_b the bulk concentrations of electrons and holes, respectively, Δ_n the ratio of photoinduced minority carriers to bulk minority carriers, also known as the injection ratio, e the magnitude of the electron charge, and k the Boltzmann constant. The space charge under equilibrium conditions Q_{sc} may be obtained by setting $\Delta_n=0$ in Eq. (2) or by using the depletion approximation as long as the equilibrium surface is indeed depleted.

The equilibrium surface-state charge per unit area is given by[23]

$$Q_{ss}=eN_t\left[\frac{1}{1+e^{eV_0-E_t/kT}}\right], \tag{3}$$

where the surface states are assumed to be donorlike, N_t is the surface-state density per unit area, E_t the surface-state energy, and V_0 the equilibrium surface potential, with E_t and V_0 measured with respect to the bulk Fermi level. The surface-state charge *may* change as the surface potential shifts due to illumination. Nonequilibrium surface-state charge may be treated either as fixed, $Q_{ss}=Q_{ss}^*$, or as varying with surface Fermi level position, $Q_{ss}\neq Q_{ss}^*$, corresponding to long and short lifetime traps, respectively. For a varying surface-state charge, V^* should replace V_0 in Eq. (3) to describe nonequilibrium surface-state charge Q_{ss}^*. For nonvarying surface-state charge, Eq. (3) describes both equilibrium and nonequilibrium surface-state charge. The surface-state charge in the current work was assumed to be constant, i.e., $Q_{ss}=Q_{ss}^*$, based on the fairly slow SPV decay, which in the current study occurred over ~10 min. A more detailed study of surface potential transients was beyond the scope of the current work, but such transients have been previously investigated[6] and modeled by a thermionic decay mechanism with a time varying barrier. Allowing surface-state charge to vary during the illumination-induced surface potential shifts would simply result in somewhat smaller predicted SPV values. This may be understood by considering a *p*-type surface. As surface band bending decreases due to illumination, surface states would move above the Fermi level, increasing the positive charge in the surface states and therefore partially compensating the photoinjected minority carrier electrons. The expected SPV trends as a function of acceptor concentration would, however, remain the same.

Under equilibrium conditions, the surface potential V_0, and therefore Q_{ss}, are uniquely defined for a given surface-state density, energy, and ionized dopant density N_A by imposing charge neutrality. For equilibrium conditions, substituting surface state and surface depletion charge expressions, given by Eq. (3) and the depletion approximation, respectively, into Eq. (1) gives

$$eN_t\left[\frac{1}{1+e^{V_0-E_t/kt}}\right]-\sqrt{\frac{2\varepsilon_s N_A V_0}{e}}=0, \tag{4}$$

allowing for the extraction of V_0, and by simple extension using Eq. (3), Q_{ss}. For the current simulations, the initial band bending is defined by an assumed surface-state density and energy of 2×10^{13} cm^{-2} and 1.5 eV,[24] respectively. Changes in these values have little qualitative influence on the resulting behavior,[25] i.e., SPV trends versus injection ratio and doping remain the same. Ionized dopants in the depletion region are estimated to be 50% of the total Mg

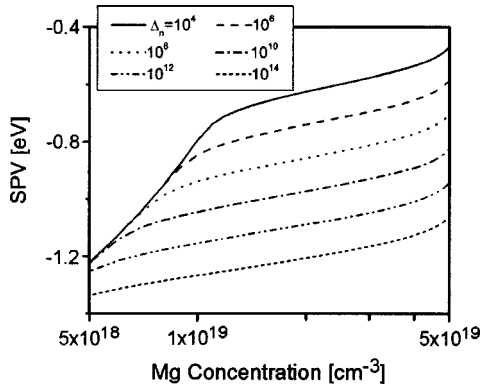

FIG. 6. Predicted photovoltage response (SPV) plotted as a function of Mg concentration for several injection ratios Δ_n. Decreased ionized impurity concentration results in increased SPV magnitude.

concentration based on previous capacitance-voltage studies[26] of Mg-doped GaN grown by MOCVD. The initial surface potential V_0 is extracted from Eq. (4), and then used to obtain surface charge Q_{ss} from Eq. (3). The surface-state charge Q_{ss} and the nonequilibrium surface depletion charge defined by Eq. (2) are then substituted into Eq. (1) allowing for the extraction of the nonequilibrium surface potential V^*, and then surface photovoltage since $\mathrm{SPV}=V^*-V_0$.

The calculated SPV response is plotted in Fig. 6 as a function of Mg concentration and for several injection ratios. As is evident from the figure, predicted SPV values were negative and increase in magnitude for increased injection ratio Δ_n. This makes intuitive sense, as injected negative charge reduces the amount of negative space charge needed to maintain neutrality with the positive surface charge. A larger amount of injected negative charge results in a greater reduction of the space charge required for charge neutrality and therefore a greater shift in surface depletion width and band bending upon illumination. One may also see that the magnitude of the predicted SPV increases with decreasing Mg concentration. This occurs because for a given concentration of injected charge, a corresponding shift in depletion layer charge is needed to maintain charge neutrality. To accommodate these charge requirements, materials with decreased ionized dopant concentration will exhibit a greater shift in depletion width and therefore, surface potential. The magnitudes of the predicted SPV values plotted in Fig. 6 are somewhat larger than those observed and presented in Fig. 4. This may be due to smaller injection ratios or a variation of surface-state charge under nonequilibrium conditions as discussed previously, both of which would decreased SPV magnitude; however, the exhibited trends would remain the same and therefore do not alter the implications of our calculations.

These results demonstrate that variations in background dopant concentration can give rise to substantial SPV variations and that other possible sources of SPV variation in these samples are unlikely to be present. Specifically, regions of decreased acceptor concentration will demonstrate increased SPV response. In addition, these same regions would be expected to exhibit decreased reverse-bias current flow due to increased surface depletion layer widths and reduced carrier concentrations. Therefore, decreased dopant concentration would cause both decreased conductivity and increased SPV, both of which are observed and closely correlated with dislocations in the *p*-type samples under investigation. This correlation is consistent with reduced Mg concentration near dislocations. As mentioned previously, TEM measurements[7] have provided evidence of Mg segregation to dislocation cores leading to a decreased density of active Mg acceptors in the vicinity of dislocations. We therefore suggest that the observed decreased conductivity and increased SPV near dislocations are due to reduced Mg concentration.

IV. CONCLUSIONS

Local conductivity, surface potential, and surface photovoltage measurements were carried out on Mg-doped *p*-type GaN. Regions of reduced current, observed for both forward- and reverse-bias conditions, were correlated with the presence of threading dislocations. Although equilibrium surface potential measurements showed little variation, photovoltage response exhibited significant spatial nonuniformity over the sample surface. C-AFM and SPV measurements of the same area revealed that the presence of dislocations is correlated with regions that exhibit both decreased conductivity and increased SPV. This correlated behavior is explained as being a consequence of Mg segregation to dislocation cores, leaving Mg-poor regions surrounding dislocations. Analytical treatment of the SPV effect confirms that reduced ionized dopant concentration would lead to enhanced SPV.

ACKNOWLEDGMENTS

Part of this work was supported by the DARPA WBGS initiative (Dr. Edgar Martinez, program monitor) and by NSF (Award No. DMR0072912).

[1] S. Strite and H. Morkoc, J. Vac. Sci. Technol. B **10**, 1237 (1992).
[2] D. Seghier and H. P. Gislason, J. Appl. Phys. **88**, 6483 (2000).
[3] G. Martinez-Criado, A. Cros, A. Cantarero, N. V. Joshi, O. Ambacher, and M. Stutzmann, Solid-State Electron. **47**, 565 (2003).
[4] H. Alves, M. Böhm, A. Hofstaetter, H. Amano, S. Einfeldt, D. Hommel, D. M. Hofmann, and B. K. Meyer, Physica B **308–310**, 38 (2001).
[5] I. Shalish, L. Kronik, G. Segal, Y. Rosenwaks, and Y. Shapira, Phys. Rev. B **59**, 9748 (1999).
[6] G. Koley, H.-Y. Cha, C. I. Thomas, and M. G. Spencer, Appl. Phys. Lett. **81**, 2282 (2002).
[7] D. Cherns, Y. Q. Wang, R. Liu, and F. A. Ponce, Appl. Phys. Lett. **81**, 4541 (2002).
[8] E. J. Miller, D. M. Schaadt, E. T. Yu, C. Poblenz, C. Elsass, and J. S. Speck, J. Appl. Phys. **91**, 9821 (2002).
[9] A. K. Henning, T. Hochwitz, J. Slinkman, J. Never, S. Hoffman, P. Kaszuba, and C. Daghlian, J. Appl. Phys. **77**, 1888 (1995).
[10] M. Nonnenmacher, M. P. O'Boyle, and H. K. Wickramasinghe, Appl. Phys. Lett. **58**, 2921 (1991).
[11] L. Kronik and Y. Shapira, Surf. Sci. Rep. **37**, 1 (1999).
[12] B. Heying, E. J. Tarsa, C. R. Elsass, P. Fini, S. P. Denbaars, and J. S. Speck, J. Appl. Phys. **85**, 6470 (1999).
[13] P. J. Hansen, Y. E. Strausser, A. N. Erickson, E. J. Tarsa, P. Kozodoy, E. G. Brazel, J. P. Ibbetson, U. Mishra, V. Narayanamurti, S. P. Denbaars, and J. S. Speck, Appl. Phys. Lett. **72**, 2247 (1998).
[14] G. Koley and M. G. Spencer, Appl. Phys. Lett. **78**, 2873 (2001).
[15] D. Zakharov and Z. Liliental-Weber (unpublished).
[16] B. Beaumont, P. Gibart, M. Vaille, S. Haffouz, G. Nataf, and A. Bouillé, J. Cryst. Growth **189**, 97 (1998).

[17] H. M. Ng, D. Doppalapudi, T. D. Moustakas, N. G. Weimann, and L. F. Eastman, Appl. Phys. Lett. **73**, 821 (1998).
[18] B. S. Simpkins, E. T. Yu, P. Waltereit, and J. S. Speck, J. Appl. Phys. **94**, 1448 (2003).
[19] J. W. Hsu, M. J. Manfra, R. J. Molnar, B. Heying, and J. S. Speck, Appl. Phys. Lett. **81**, 79 (2002).
[20] H. O. Jacobs, P. Leuchtmann, O. J. Homan, and A. Stemmer, J. Appl. Phys. **84**, 1168 (1998).
[21] Y. K. Hsieh and H. C. Card, J. Appl. Phys. **65**, 2409 (1989).
[22] D. R. Frankl, Surf. Sci. **3**, 101 (1965).
[23] J. S. Blakemore, *Semiconductor Statistics*, 2nd ed. (Dover, Pulications, New York, 1987) p. 81.
[24] C. I. Wu and A. Kahn, J. Appl. Phys. **86**, 3209 (1999).
[25] E. O. Johnson, Phys. Rev. **111**, 153 (1958).
[26] L. S. Yu, L. Jia, D. Qiao, S. S. Lau, J. Li, J. Y. Lin, and H. X. Jiang, IEEE Trans. Electron Devices **50**, 292 (2003).